Properties of drift waves in a filamentary density depletion

J. R. Peñano, G. J. Morales, and J. E. Maggs
Department of Physics and Astronomy, University of California, Los Angeles, Los Angeles, California 90095

(Received 26 September 1996; accepted 3 December 1996)

This analytical and numerical study explores the properties of electrostatic, drift-wave eigenmodes trapped within a magnetic field-aligned depletion in plasma density and temperature whose transverse dimension is on the order of the electron skin depth. The dependence of the complex eigenfrequencies on key parameters is investigated for collisionless and collisional plasma. The collisional description is based on the Lorentz model of electron pitch-angle scattering. The separate roles of the gradients in density and temperature are illustrated for the collisional and collisionless regimes. The predictions are compared to experimental observations [J. E. Maggs and G. J. Morales, Geophys. Res. Lett. **23**, 633 (1996); Phys. Plasmas **4**, 290 (1997)] of a controlled striation in the laboratory. © *1997 American Institute of Physics.* [S1070-664X(97)01303-7]

I. INTRODUCTION

The properties of electrostatic drift waves have been extensively investigated[1] theoretically and experimentally, primarily motivated by the effect that these modes can have on the confinement characteristics[2] of strongly magnetized plasmas. Because of this overwhelming interest, the majority of the studies have focused on drift waves excited near the edge of macroscopic plasmas having a relatively gentle gradient of plasma density and temperature. In describing such an environment it has been common to use a local analysis in which the radial mode structure is ignored and the difficulties associated with the outer radial boundary conditions are bypassed. However, detailed studies[3,4] have also found the differences between the predictions of a radial eigenmode analysis and those of local theory to be substantial. In both approaches a conceptual difficulty complicates the comparison of theoretical predictions to experimental observations, i.e., how to describe the zeroth-order plasma profiles in contact with the surrounding vessel. In contrast to the edge-plasma studies of drift waves, in the present investigation we focus on the behavior associated with a microscopic depletion in density and temperature embedded within an infinite plasma and aligned with the confining magnetic field (i.e., a filament or striation). By microscopic it is meant that the radial scale length is comparable to the electron skin depth, c/ω_{pe}, where c is the speed of light and ω_{pe} is the electron plasma frequency. The ions are considered to be sufficiently cold, so that the Larmor radius ρ_i is much smaller than the scale length of the striation. This configuration provides a paradigm for the study of drift-wave eigenmodes because the radial boundary condition is well posed, i.e., the fields are asymptotically evanescent in the radial direction and no interaction with a material wall occurs.

The broader interest in exploring the properties of drift waves in microscopic filaments is that, increasingly, it is being recognized[5–11] that filamentary structures are a fundamental feature of magnetized plasmas that are far from thermal equilibrium. Specifically, density depletions of the type investigated in this study have been observed in widely different environments including ionospheric heating experiments,[12] *in situ* measurements of the auroral ionosphere by rockets[13] and spacecraft,[14] and in radar and rocket studies[15] of the equatorial F region. Of course, density depletions are also a direct consequence of nonlinear changes caused by ponderomotive forces and filamentation instabilities. The spontaneously generated drift waves can give rise to localized ion heating and electron acceleration, and also determine the lifetime of the striations.

The goals of the present analytical and numerical study are two-fold: (1) to delineate the general properties of drift waves trapped within narrow striations, (2) to provide a quantitative comparison with experimental observations[16,17] of a controlled striation generated in the Large Plasma Device[18] (LAPD) at the University of California, Los Angeles (UCLA). The present analysis is extremely valuable in providing a framework for understanding the complex behavior of the fluctuations observed in the laboratory study. The reason is that the experiment encompasses at least three regimes: pure drift waves, drift-Alfvén waves, and pure Alfvén waves, together with possible nonlinearities and couplings. Thus, the present restricted study is meant to identify those features in the experiment that are a direct consequence of the physics associated with electrostatic drift waves. Future studies will address the Alfvénic fluctuations and the role of nonlinearities.

This paper is organized as follows. In Sec. II a formulation of the radial eigenvalue problem is obtained for (a) the collisionless regime, and (b) collisional plasma described by a Lorentz model. In Sec. III we explore numerical solutions of the eigenvalue problem to deduce dependences on key physical parameters for the collisionless and collisional regimes. A quantitative comparison to the LAPD experimental observations is made in Sec. IV and a discussion of the results is presented in Sec. V.

II. FORMULATION

A. Collisionless regime

First we proceed to obtain a differential equation describing the linear behavior of electrostatic drift waves, trapped within a striation, in the absence of collisions. In describing the kinetic response of the collisionless plasma

we use notation that will prove to be convenient for describing the collisional plasma. Cylindrical geometry (r,θ,z) is used with the z axis along the confining magnetic field whose magnitude is B. The striation is assumed to be azimuthally symmetric with a radial density profile $n_0(r)$ and a corresponding electron temperature profile $T_e(r)$. For simplicity in this study we ignore the effect of a zeroth-order (dc) electric field with the understanding that there exist important features related to the shear in azimuthal flow. Because of the subtleties involved, however, these effects are deferred to a separate investigation.

The low-frequency response ($\omega \ll \Omega_i$, where Ω_i is the ion cyclotron frequency) associated with small-amplitude, electrostatic drift waves in a plasma in which the Larmor radius of all species is much smaller than the scale length of all relevant quantities is well described by the linearized drift-kinetic equation,[19] which in the collisionless limit takes the form

$$\frac{\partial}{\partial t} f_j + v_\parallel \frac{\partial}{\partial z} f_j + \nabla_\perp \cdot (\mathbf{v}_\perp f_{0j}) + \frac{q_j}{m_j} E_\parallel \frac{\partial}{\partial v_\parallel} f_{0j} = 0, \tag{1}$$

with the transverse low-frequency velocities given by

$$\mathbf{v}_\perp = \frac{\mathbf{E}\times\hat{z}}{B} c + \frac{m_j c^2}{q_j B^2} \left(\frac{\partial}{\partial t} \mathbf{E}_\perp + v_\parallel \frac{\partial}{\partial z} \mathbf{E}_\perp \right), \tag{2}$$

where f_{0j} is the zeroth-order distribution function of species j having charge and mass q_j and m_j, respectively. The linearly perturbed distribution is f_j and the self-consistent fluctuating field is electrostatic, i.e., $\mathbf{E} = -\nabla\phi$. All fluctuating quantities are assumed to have the functional form (e.g., the potential)

$$\phi(\mathbf{r},t) = \tilde{\phi}(r) \exp[\iota(k_\parallel z + \ell\theta - \omega t)] + \text{c.c.} \tag{3}$$

The zeroth-order electron distribution is taken to be representative of that measured in the laboratory, i.e., a stationary Maxwellian with radially dependent density, $n_0(r)$, and thermal velocity, $\overline{v_e}(r) = \sqrt{T_e(r)/m}$, where m is the electron mass.

Solving Eq. (1) for f_e and integrating over the parallel velocity $v_\parallel$ results in the fluctuating electron density

$$\tilde{n}_e(r) = -\frac{mc^2}{eB^2}\left[\frac{1}{r}\frac{\partial}{\partial r}\left(r n_0 \frac{\partial \tilde{\phi}}{\partial r} \right) - \frac{\ell^2}{r^2}\tilde{\phi} n_0 \right] - \frac{e\tilde{\phi}}{m\overline{v_e^2}} n_0 \frac{Z'(\zeta_e)}{2} + \frac{\ell}{r}\frac{c\tilde{\phi}}{\omega B}\frac{\partial}{\partial r}[n_0 \zeta_e Z(\zeta_e)], \tag{4}$$

where $\zeta_e(r) \equiv \omega/[\sqrt{2} k_\parallel \overline{v_e}(r)]$ is the scaled, complex phase velocity. Here $Z[\xi_e(r)]$ represents the collisionless plasma dispersion function and $Z'[\zeta_e(r)]$ is the derivative with respect to $\zeta_e(r)$. Also, e is the quantum of charge.

The ion density fluctuation $\tilde{n}_i$ is obtained in a similar manner, but since the ions are assumed to be relatively cold, the corresponding functions $Z(\zeta_i)$ and $Z'(\zeta_i)$ are expanded in the limit of a large argument. To incorporate a damping experienced by large ℓ-number modes, the effect of ion viscosity associated with shear in the fluctuating $\mathbf{E}\times\mathbf{B}$ azimuthal flow is included. This results in

$$\tilde{n}_i(r) = \frac{Mc^2}{eB^2}\left[\frac{1}{r}\frac{\partial}{\partial r}\left(r n_0 \frac{\partial \tilde{\phi}}{\partial r} \right) - \frac{\ell^2}{r^2}\tilde{\phi} n_0 - \iota \frac{\eta}{M\omega}\left(\frac{\ell}{r}\right)^4 \tilde{\phi} \right] + \frac{e n_0}{M}\frac{k_\parallel^2}{\omega^2}\tilde{\phi} - \left(\frac{\ell}{r}\right)\frac{c\tilde{\phi}}{\omega B}\frac{\partial n_0}{\partial r}, \tag{5}$$

for singly charged ions of mass M, where

$$\eta = \frac{3 n_0 T_i}{10 \Omega_i^2 \tau_i}, \tag{6}$$

is the viscosity coefficient calculated by Braginski[20] with

$$\tau_i = \frac{3\sqrt{M} T_i^{3/2}}{4\sqrt{2\pi} n_0 \Lambda e^4}, \tag{7}$$

the ion collision time. Here Λ is the Coulomb logarithm and T_i the ion temperature.

Neglecting the vacuum term in Poisson's equation (i.e., setting $\tilde{n}_e \approx \tilde{n}_i$) results in a differential equation that governs the eigenvalue problem. In terms of scaled quantities it takes the form

$$\frac{1}{\rho N(\rho)}\frac{\partial}{\partial \rho}\left(\rho N(\rho)\frac{\partial}{\partial \rho}\tilde{\phi} \right) + V(\rho, W)\tilde{\phi} = 0, \tag{8}$$

where

$$V(\rho, W) = \left(\frac{K^2}{W^2} + \frac{Z_N(W,\rho)}{2T(\rho)} \right)\lambda^2 - \left(\frac{\ell}{\rho}\right)^2 - \frac{\iota\overline{\eta}}{\lambda^2 W}\left(\frac{\ell}{\rho}\right)^4 + \left(\frac{\ell}{\rho}\right)\frac{\Gamma(W,\rho)}{W}, \tag{9}$$

plays the role of an effective potential.

The quantity

$$\Gamma(W,\rho) = \frac{1}{2}\left(Z_N(W,\rho)\frac{\partial}{\partial \rho}\ln N(\rho) + Z_T(W,\rho)\frac{\partial}{\partial \rho}\ln T(\rho) \right), \tag{10}$$

contains the effects of the density and temperature gradients responsible for the instability of the drift waves.

The useful scaled quantities are

$$W = \frac{\omega}{\Omega_i}; \quad \rho = \frac{r}{L_N}; \quad K = \frac{k_\parallel c_s}{\Omega_i}; \quad \lambda = \frac{L_N \Omega_i}{c_s}; \quad \overline{\eta} = \frac{3}{10}\frac{T_i}{T_e(0)}\frac{1}{\Omega_i \tau_i}, \tag{11}$$

with $N(\rho) = n_0(\rho)/n_0(0)$ and $T(\rho) = T_e(\rho)/T_e(0)$ representing the scaled density and electron temperature profiles. The sound speed at the center of the striation is $c_s = [T_e(0)/M]^{1/2}$. Here L_N is the characteristic scale length of the density profile of the striation (on the order of the electron skin depth) and is chosen as the scaling length for the radial distance. Of course, the temperature profile has its own scale length L_T, but in the present problem it is also on the order of c/ω_{pe}. The small ion temperature entering in the viscosity coefficient is taken to be spatially uniform.

The functions Z_N and Z_T appearing in Eq. (10) describe the kinetic response of electrons corresponding to the gradients in density and temperature, respectively. In this collisionless formulation these functions are simply related to the usual plasma dispersion function, i.e.,

$$Z_N \rightarrow Z'(\zeta_e), \tag{12}$$

$$Z_T \rightarrow -\frac{\zeta_e Z''(\zeta_e)}{2}. \tag{13}$$

Next it is shown that for a collisional plasma, the form of the eigenvalue differential equation is the same as given by Eqs. (8)–(9), but with the functions Z_N and Z_T replaced by their collisional counterparts.

B. Collisional plasma

The collisional process having the largest effect on the linear properties of drift waves is electron pitch-angle scattering because it determines the ability of electrons to short out potential fluctuations by streaming along the magnetic field. We describe this effect by including a Lorentz collision operator in the drift-kinetic equation for electrons following the procedure developed by Koch and Horton.[21] Equation (1) then takes the form

$$\frac{\partial}{\partial t} f_e + v_\parallel \frac{\partial}{\partial z} f_e + \nabla_\perp \cdot (\mathbf{v}_\perp f_{0e}) - \frac{e}{m} E_\parallel \frac{\partial}{\partial v_\parallel} f_{0e} = -\nu(v,r) \frac{\partial}{\partial \mu}\left((1-\mu^2) \frac{\partial f_e}{\partial \mu} \right), \tag{14}$$

where $\nu(v,r) = -\nu_e (\sqrt{2}\overline{v_e}/v)^3$ and $\nu_e = 2\pi n_0 e^4 \Lambda / [m^2 (\sqrt{2}\overline{v_e})^3]$ is the electron–ion collision frequency. The quantity μ represents the cosine of the velocity pitch angle and v is the magnitude of the velocity.

The perturbed distribution function is expanded in Legendre polynomials $P_n(\mu)$,

$$f_e = \sum_{n=0}^{\infty} a_n(v) P_n(\mu), \tag{15}$$

from which it follows that the fluctuating electron density is given by

$$\tilde{n}_e = 4\pi \int_0^\infty dv\ v^2 a_0(v). \tag{16}$$

The important coefficient, a_0, is determined by inserting Eq. (15) into (14) to generate a recursion relation that results in a continued fraction representation,

$$a_0 = \frac{\iota A_0}{\omega} + \frac{\overline{A_0}}{-\iota\omega - 2\nu(v,r) + (\iota k_\parallel^2 v^2/3\omega) + \frac{2}{5}\iota k_\parallel v (a_2/a_1)}, \tag{17}$$

where

$$A_0 = \iota \left(\frac{\mathscr{E}}{\rho}\right) \frac{c\tilde{\phi}}{B} \frac{\partial}{\partial r} f_{0e} + \frac{mc^2}{eB^2} \iota\omega \left[\frac{1}{r} \frac{\partial}{\partial r}\left(r f_{0e} \frac{\partial \tilde{\phi}}{\partial r} \right) - \left(\frac{\mathscr{E}}{\rho}\right)^2 f_{0e} \tilde{g} f \right], \tag{18}$$

$$\overline{A_0} = \frac{k_\parallel v}{3\omega} \left[\iota k_\parallel v \frac{e\tilde{\phi}}{m\overline{v_e^2}} f_{0e} + \iota \left(\frac{\mathscr{E}}{\rho}\right) \frac{c\tilde{\phi}}{B} \frac{k_\parallel v\ \partial}{\omega\ \partial r} f_{0e} \right]. \tag{19}$$

The ratio a_2/a_1 corresponds to a continued fraction defined by

$$\frac{a_n}{a_{n-1}} = \frac{-b_n}{d_n + b_{n+1}(a_{n+1}/a_n)}, \tag{20}$$

where

$$b_n = \frac{\iota k_\parallel v n}{(2n-1)(2n+1)}; \quad d_n = -\frac{\iota\omega + \nu(v,r) n(n+1)}{2n+1}. \tag{21}$$

The continued fraction approach is useful in the limit of strong collisionality because the iteration converges rapidly. Unfortunately, convergence is very slow as ν_e is made small. In the calculations presented here Z_N and Z_T are computed using an iterative technique based on Eq. (20). In evaluating the continued fraction, a_7/a_6 and all higher-order iterations are taken to be zero. For the parameters surveyed in this paper, the maximum error in Z_N and Z_T associated with this truncation is on the order of 10^{-5}.

The terms responsible for the collisional instability of drift waves arise from the velocity integration of the term in A_0 proportional to $\partial f_{0e}/\partial r$, i.e., the gradient effects. Collecting the results of the integration and separating the terms proportional to the logarithmic derivatives of density and temperature allows the identification of the kinetic response functions equivalent to those of the collisionless regime given in Eq. (10), i.e., now

$$\begin{pmatrix} Z_N \\ Z_T \end{pmatrix} \rightarrow \frac{-8}{\sqrt{\pi}} \int_0^\infty \frac{dt\ t^2 \exp(-t^2)}{D(t,\rho)} \begin{pmatrix} 1 \\ t^2 - \frac{3}{2} \end{pmatrix}, \tag{22}$$

where

$$D(t,\rho) = 1 - \frac{3\zeta_e^2}{t^2} + \frac{\iota 6 \overline{\nu}\zeta_e}{t^5} + \frac{6\zeta_e}{5t}\left(\frac{a_2}{a_1}\right), \tag{23}$$

and $\overline{\nu} = \nu_e/[\sqrt{2} k_\parallel \overline{v_e}(\rho)]$ is the scaled collision frequency.

The factor $t^2 - \frac{3}{2}$ associated with the temperature gradient arises from the radial derivative of the normalized zeroth-order distribution function, i.e., the term

$$\frac{\partial}{\partial r}\left(\frac{\exp[-mv^2/2T_e(r)]}{[T_e(r)]^{3/2}} \right). \tag{24}$$

The terms in a_0 not proportional to $\partial f_{0e}/\partial r$ result in a contribution that is proportional to Z_N. Thus, this function plays the same role as the function Z' in the collisionless parallel dielectric, but now for a collisional plasma. With these results it is seen that the differential equation describing the collisional eigenvalue problem has the same form as Eqs. (8)–(10) with the replacement of Z_T and Z_N given by Eq. (22). Of course, these results refer to the electron dynamics so the ion response is treated the same as in the collisionless regime.

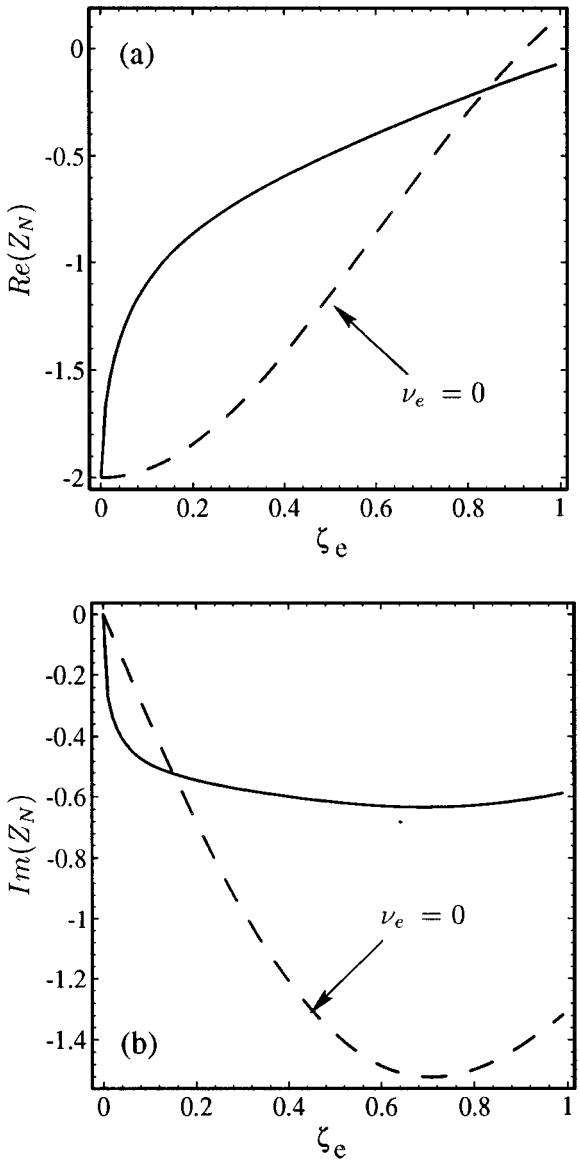

FIG. 1. Dependence on scaled parallel phase velocity of the kinetic response function Z_N associated with a gradient in plasma density for the collisionless regime [Eq. (13)] and collisional plasma [Eq. (22)] for parameters corresponding to the LAPD experiment.

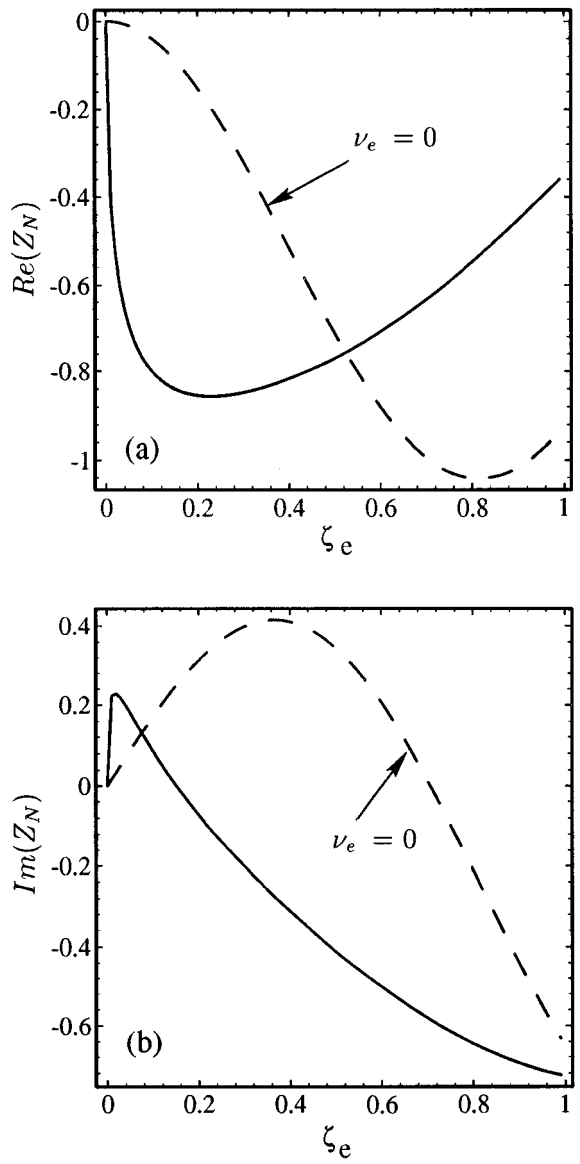

FIG. 2. Dependence on scaled parallel phase velocity of the kinetic response function Z_T associated with a gradient in electron temperature for the collisionless regime [Eq. (13)] and collisional plasma [Eq. (22)] for parameters corresponding to the LAPD experiment.

To better appreciate the distinction between the collisionless and collisional response of electrons to drift waves, Figs. 1 and 2 display the behavior of the real and imaginary parts of Z_N and Z_T for parameters characteristic of the LAPD experiment ($n_0=1.4\times10^{12}$, $T_e=10$ eV, $k_\parallel=\pi/L$, $L=10^3$ cm). In general, the range of parameters relevant to the experiment correspond to $\zeta_e<0.6$. Figure 1(a) shows that for $\zeta_e<0.8$ collisions prevent the electrons from achieving the adiabatic response characterized by $\mathrm{Re}(Z_N)=-2$. In fact, over a significant range of parameters relevant to the drift waves the magnitude of the collisional $\mathrm{Re}(Z_N)$ is a factor of 2 smaller than the collisionless result. Quantitatively, this causes the frequency of the collisional modes to be lower than in the collisionless regime. Also, because the electron response is not adiabatic, corrections to the electron diamagnetic drift frequency arising from a finite parallel wave number are important over a wider range of parameters.

It is seen from Fig. 1(b) that over the range $0.2<\zeta_e<1$ collisions reduce the magnitude of $\mathrm{Im}(Z_N)$, i.e., collisions actually help the electrons to short out the fluctuations by providing a decorrelation to the strong wave–particle interaction. This causes the drift waves to experience a reduced growth rate at longer wavelengths. However, in the region $\zeta_e<0.1$ the collisionless contribution is smaller than the collisional one, thus implying a broadening of the growth rate as the parallel wave number is increased.

Figure 2(a) indicates that for lower phase velocities ($\zeta_e<0.5$) collisions increase the magnitude of $\mathrm{Re}(Z_T)$. This property causes the real part of a drift wave eigenfrequency in a collisionless plasma having a temperature gradient to become larger than that in the collisionless region as $k_\parallel$ is increased. This trend, however, is reversed for $\zeta_e>0.5$, as

may be appropriate for striations having very large temperature gradients.

Figure 2(b) shows that in the collisionless regime $\mathrm{Im}(Z_T)>0$ for $\zeta_e<0.7$. This implies that a temperature gradient in the same direction as the density gradient reduces the growth rate of waves excited due to $\mathrm{Im}(Z_N)<0$. In the limiting case in which $\nabla n_0=0$, temperature gradient drift waves can only arise for $\zeta_e>0.7$, as is consistent with the computer simulations of Tokuda *et al.*[22] for collisionless systems.

However, in a collisional plasma this behavior is significantly changed. As is seen in Fig. 2(b) the region over which $\mathrm{Im}(Z_T)>0$ is limited to $\zeta_e<0.18$, where, in fact, the amplitude of $\mathrm{Im}(Z_T)$ is significantly increased over the collisionless value. The consequences of this behavior for the collisional plasma is that a temperature gradient in the same direction as a density gradient enhances the growth for $\zeta_e>0.18$ and reduces the growth of modes with lower values.

III. NUMERICAL RESULTS

In surveying the properties of the unstable drift waves, it is useful to consider first the predictions of a local analysis, i.e., setting $V(W,\rho)=0$. As is well known, there exist two (asymptotically different) modes supported in this low-frequency regime: a weakly damped ion acoustic wave unaffected by the plasma gradients and approximately given by

$$\frac{K^2}{W^2}\simeq -\frac{1}{2}Z_N, \quad K^2\gg\left(\frac{\ell}{\rho}\right)W\Gamma, \tag{25}$$

and the drift wave of interest,

$$W\simeq \frac{(\ell/\lambda^2\rho)\Gamma-\iota(\ell/\lambda\rho)^4\overline{\eta}}{-(Z_N/2T(\rho))+(\ell/\lambda\rho)^2}, \quad K^2\ll\left(\frac{\ell}{\rho}\right)W\Gamma, \tag{26}$$

which can be unstable through the gradient terms contained in Γ, which are proportional to $\mathrm{Im}(Z_N)$ and $\mathrm{Im}(Z_T)$.

Numerically solving the dispersion relation $V(W,\rho)=0$ for the drift wave root of an $\ell=1$ mode at every radial position, for the density and temperature profiles measured in the LAPD experiment, results in the values of the wave frequency ($\omega/2\pi$) and growth rate γ shown in Fig. 3. As expected, it is seen that the largest growth rate arises near the location of the steepest gradient while near the origin, strong damping results due to viscous dissipation associated with the short-scale structure. The frequency corresponding to the largest growth rate is approximately 80 kHz, which is a factor of 2 larger than observed in the laboratory, thus indicating the limitations associated with a local analysis.

For completeness it should be mentioned that the parameters used in generating Fig. 3 correspond to conditions for which experimental observations exist, namely a singly ionized helium plasma confined by a 1 kG magnetic field with a uniform ion temperature of 0.6 eV. The density striation has a contrast of $n_0(\infty)/n_0(0)=3.7$ with $n_0(0)=7\times10^{11}$ cm^{-3}, and an associated electron temperature contrast $T_e(\infty)/T_e(0)=1.9$ with $T_e(0)=6$ eV. The value of $k_\parallel$ corresponds to the largest axial wavelength that can fit into the LAPD device, i.e., $2\pi/k_\parallel=20$ m.

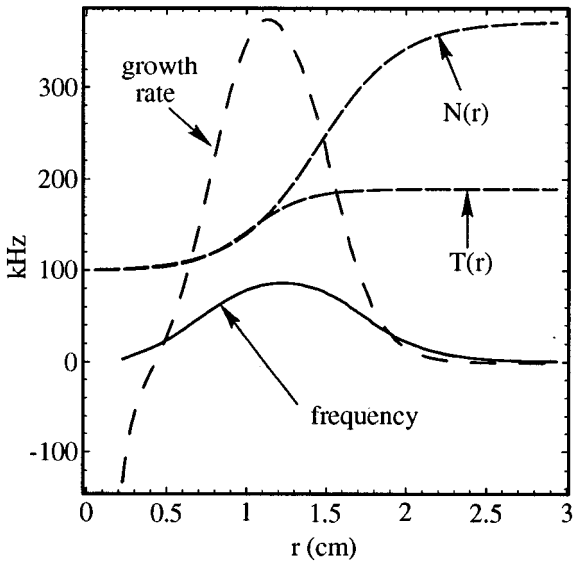

FIG. 3. Predictions of local theory for a ($\ell=1$, $k_\parallel=\pi/L$) mode corresponding to the scaled density, $N(r)$, and the scaled electron temperature, $T(r)$, measured in the LAPD experiment.

The complex eigenvalues and radial eigenfunctions of unstable drift waves trapped within a striation are obtained by solving Eqs. (8)–(10) using a numerical shooting method. To simplify the numerical procedure, the experimentally measured density and temperature profiles are fitted with hyperbolic tangent functions, which reproduce the data quite well. The temperature profiles are used to construct the radially dependent functions Z_N and Z_T, which for the relevant parameters of the collisional regime is the most tedious part of the scheme [using the continued fraction technique of Eq. (20)].

The numerical shooting method uses the asymptotic dependences

$$\tilde{\phi}(\rho\to 0)\to\rho^{\ell}\exp\left(-\frac{\ell^2}{\rho}\sqrt{\frac{\iota\overline{\eta}}{\lambda^2 W}}\right), \tag{27}$$

$$\tilde{\phi}(\rho\to\infty)\to\sqrt{\frac{2}{\iota\pi\lambda\rho}}\exp\left[\lambda\rho-\iota\frac{\pi}{2}\left(\ell+\frac{1}{2}\right)\right], \tag{28}$$

derived from the collisionless analysis [i.e., Eqs. (8)–(10)] to specify numerical values at a point ρ_0, close to the origin, and at a large distance ρ_∞ well outside the striation. Equations (8)–(10) are integrated outward by a fourth-order Runge–Kutta scheme from ρ_0 to an intermediate fitting point ρ_m and inward from ρ_∞ to ρ_m. The complex value of $\tilde{\phi}(\rho_0)$ and W is iterated until the solutions from both directions join smoothly at ρ_m. Depending on how close the initial values for $\tilde{\phi}(\rho_0)$ and W are to the solution, a typical calculation converges in four to six iterations.

Since the radial structure of the trapped electrostatic modes is experimentally obtained by measuring the fluctuations in the ion saturation current collected by a small probe, i.e., proportional to $\tilde{n}_i$, it is useful to display the results of

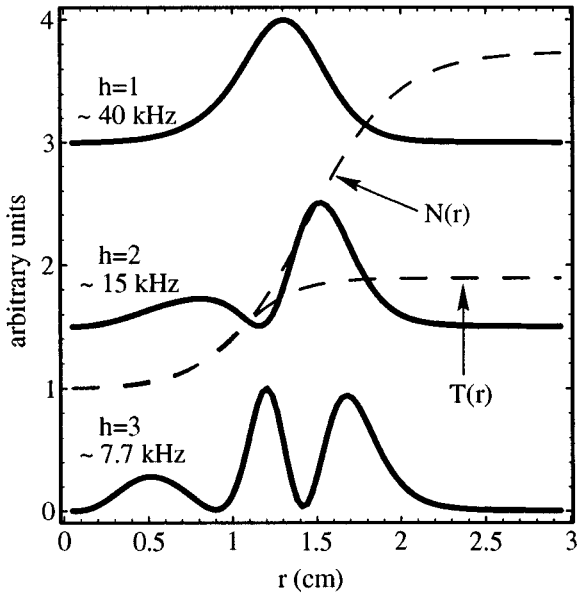

FIG. 4. Predicted radial eigenfunctions of density fluctuations for a ($\ell=1$, $k_\parallel=\pi/L$) mode. Note that the zero scale of eigenfunctions is shifted vertically for ease of display.

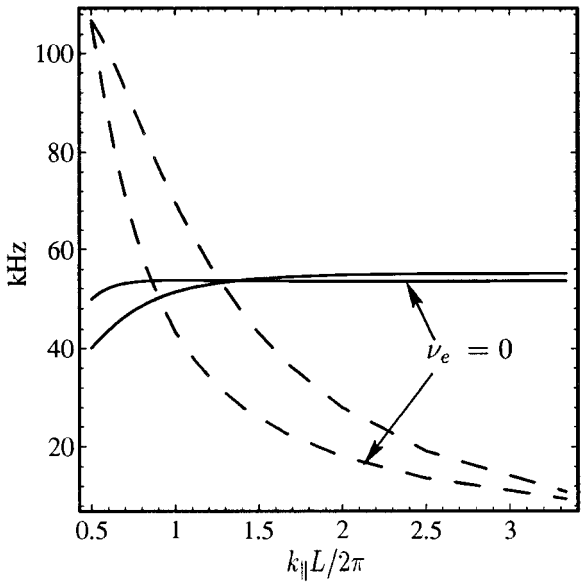

FIG. 5. Dependence on the scaled parallel wave number of the wave frequency, $\omega/2\pi$ (solid curves) and growth rate (dashed curves) of the ($\ell=1$, $h=1$) mode for the collisionless regime ($\nu_e=0$) and collisional plasma.

the eigenmode analysis in terms of this quantity. Combining Eqs. (5) and (8) results in a simple expression proportional to the potential eigenfunction,

$$\frac{\tilde{n}_i(\rho)}{n_0(\rho)} = -\left[\frac{Z_N(W,\rho)}{2T(\rho)} + \left(\frac{\ell}{\rho}\right)\frac{1}{\lambda^2 W}\left(\Gamma(W,\rho) + \frac{\partial}{\partial\rho}\ln N(\rho)\right)\right]\left(\frac{e\tilde{\phi}(\rho)}{T_e(0)}\right). \tag{29}$$

Figure 4 displays the predicted spatial pattern of $|\tilde{n}_i|^2$ associated with an $\ell=1$ mode for three different radial eigenmodes. The lowest radial eigenmode has the largest frequency ($\approx$40 kHz) and the largest growth rate ($\approx 103\times10^3$/s), which are significantly different from the estimates given by the local analysis shown in Fig. 3, obtained for the same parameters. The general trend seen from Fig. 4 is that for fixed ℓ and axial wave number $k_\parallel$ the frequency of the trapped modes decreases as the radial mode number, h, increases. Although not shown, the corresponding growth rates also decrease, as expected.

The dependence on parallel wave number of the eigenfrequency and growth rate of the ($\ell=1$, $h=1$) mode is shown in Fig. 5. Note that the wave number is scaled to the length of the device L. For comparison the collisionless results [i.e., using the Z_N and Z_T of Eqs. (13) for the same profiles] are also shown. The general trend seen is the same for both regimes: the frequency increases rapidly for smaller $k_\parallel$ values and reaches a maximum value ($<$55 kHz). In both regimes the largest growth rate corresponds to the lowest axial mode and as $k_\parallel$ increases the growth rate decreases, as expected from the behavior of Im(Z_N) shown in Fig. 1(b).

Figure 6 exhibits the dependence on parallel wave number of the frequency and growth rate of higher ℓ modes for the collisional plasma. It is seen that the $\ell=2$ and $\ell=3$ modes can have appreciably higher frequencies ($\approx$75 kHz) and growth rates than the $\ell=1$ mode at shorter axial wavelengths.

The dependence of the frequency and growth rate of the ($\ell=1$, $h=1$, $k_\parallel=\pi/L$) mode on the confining magnetic field strength, B, is shown in Fig. 7. It is seen that the frequency remains relatively constant as B is varied from 0.5 to 2 kG for both collisionless and collisional regimes. However, the collisional mode is unstable over a wider range of B than the

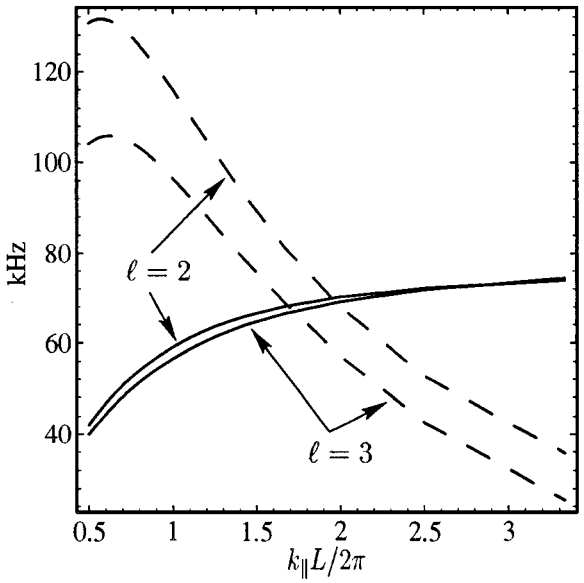

FIG. 6. Dependence on the scaled parallel wave number of the wave frequency (solid curves) and growth rate (dashed) for higher ℓ modes corresponding to the fundamental ($h=1$) radial number. The collisional case only is shown.

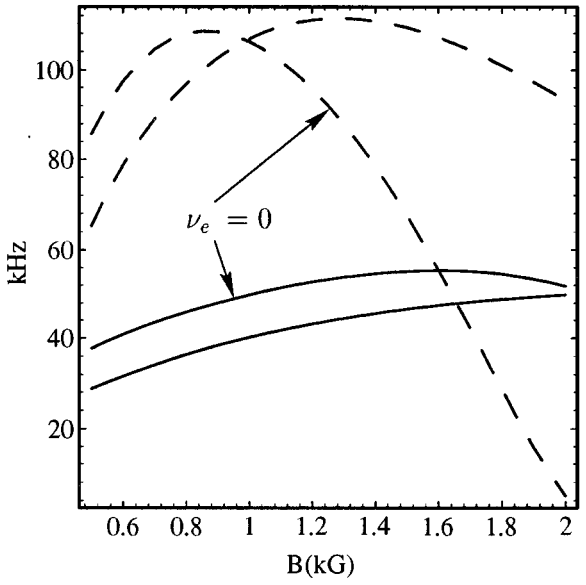

FIG. 7. Magnetic field dependence of wave frequency (solid curves) and growth rate (dashed) of the ($\ell=1$, $h=1$, $k_\parallel=\pi/L$) mode for collisionless regime ($\nu_e=0$) and collisional plasma.

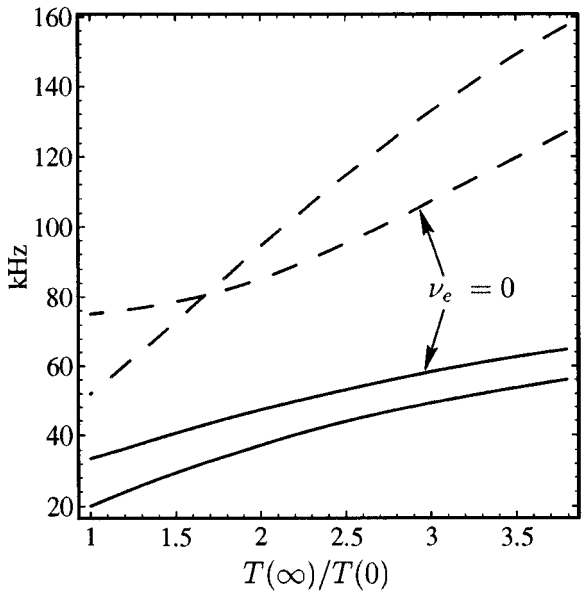

FIG. 8. The dependence on the electron temperature contrast of the wave frequency (solid curves) and growth rate (dashed) for the ($\ell=1$, $h=1$, $k_\parallel=\pi/L$) mode for a collisionless regime ($\nu_e=0$) and a collisional plasma. The density profile of the striation is held constant.

collisionless mode. This behavior is consistent with the local theory prediction of Eq. (26). The stabilization of the wave at higher magnetic fields is due to the imaginary part of Z_N in the denominator of Eq. (26). If this imaginary part is ignored, the growth rate remains positive and decreases as $1/B$ as the magnetic field is increased. The wider range of instability for the collisional plasma is due to the fact that $\mathrm{Im}(Z_T)$, for relevant phase velocities ($\zeta_e \approx 0.4$–0.5), is opposite in sign between the collisionless and collisional formulations (i.e., the temperature gradient helps to maintain the instability in the collisional plasma). Numerically it is found that the collisional mode stabilizes at $B \approx 4$ kG.

The dependence of the eigenfrequency and growth rate of the ($\ell=1$, $h=1$, $k_\parallel=\pi/L$) mode on the temperature contrast $T_e(\infty)/T_e(0)$ is shown in Fig. 8. In this survey, the temperature profile of the striation is changed and the value of $T_e(0)$ is held fixed. It is seen from Fig. 8 that there exists a substantial instability, even for a flat temperature profile. As the temperature contrast increases the growth rate also increases, but more rapidly for the collisional plasma. The eigenfrequencies increase with temperature contrast.

For the collisionless regime, the increase in the growth rate as the temperature contrast is increased can be easily misinterpreted to mean that a temperature gradient by itself can have a destabilizing effect. From Figs. 2(b) and 1(b), however, it is clear that this is not the case. The temperature gradient, in fact, helps to stabilize the wave since $\zeta_e \approx 0.5$ for the relevant parameters and in this regime $\mathrm{Im}(Z_T)>0$. As the temperature contrast is increased, ζ_e increases and the contribution of the temperature gradient to the growth rate [i.e., $\mathrm{Im}(Z_T)$] decreases while the density gradient contribution [$\mathrm{Im}(Z_N)$] increases. Thus, the increase in the growth rate is actually due to the frequency dependence of the imaginary part of Z_N, which multiplies the density gradient and is the primary driver for the instability. Furthermore, an increase in T_e will, in general, increase the growth rate. Indeed, it is this effect that is primarily responsible for the increase in the growth rate shown in Fig. 8.

The complementary dependence of the ($\ell=1$, $h=1$, $k_\parallel=\pi/L$) mode on the density contrast $n_0(\infty)/n_0(0)$ is shown in Fig. 9. Now the temperature profile is unchanged and the value of $n_0(0)$ is held fixed. For the collisionless regime the mode rapidly stabilizes as the density contrast is decreased.

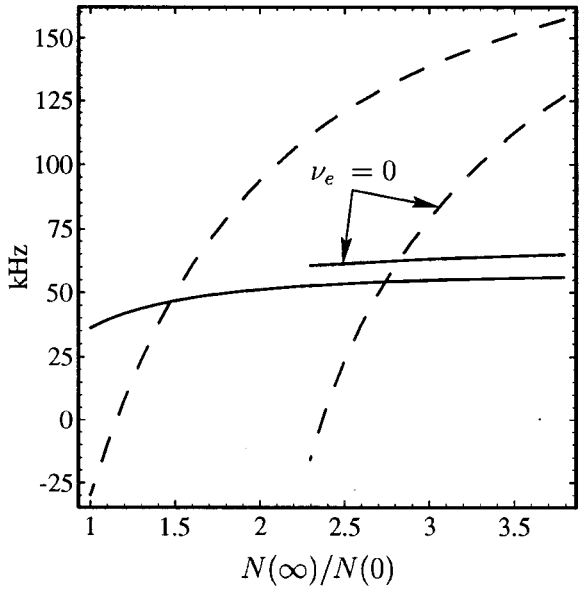

FIG. 9. Dependence on the density contrast of the wave frequency (solid curves) and growth rate (dashed) for the ($\ell=1$, $h=1$, $k_\parallel=\pi/L$) mode for a collisionless regime ($\nu_e=0$) and a collisional plasma. The electron temperature profile of the striation is held constant.

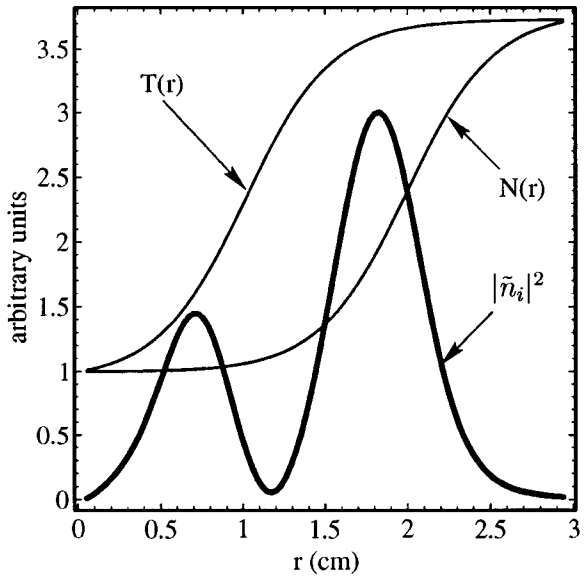

FIG. 10. The radial density eigenfunction for the lowest radial mode ($\ell=1$, $h=1$, $k_\parallel=\pi/L$) in a collisional plasma in which the positions of the largest gradients in density and electron temperature are well separated.

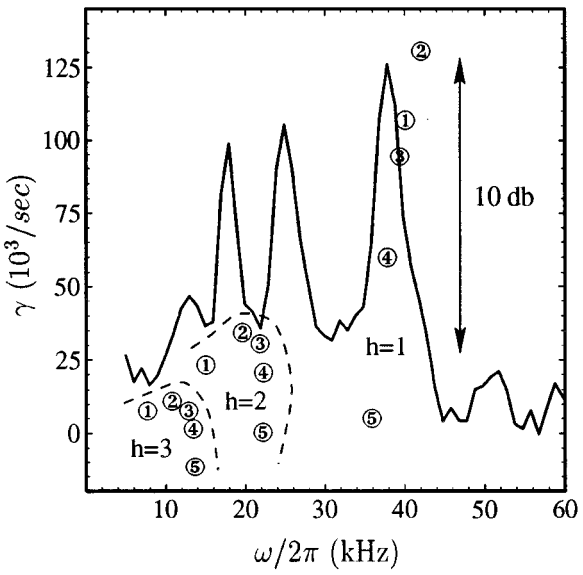

FIG. 11. A comparison of the measured spectrum (a solid curve in the log scale) to the theoretical growth rate (in the linear scale) for different combinations of (ℓ, h) mode numbers. Circles numbers label different ℓ modes. Dashed lines separate different radial modes.

The mode, is, in fact, stable in the presence of a sizable density gradient. This is due to the stabilizing effect of the temperature gradient in the collisionless regime for $\zeta_e<0.7$, as shown by Fig. 2(b). For the collisional plasma, the mode is unstable for smaller values of the density contrast, where the collisionless mode is stable. As the density contrast increases the growth rate increases sharply, but the eigenfrequencies increase slowly. In particular, it is seen that for the collisional plasma of relevance to the LAPD experiment the density contrast has no significant effect on the frequency.

Since the density and temperature gradients contribute differently to the instability of a trapped drift wave, it is worthwhile to illustrate the behavior for a striation in which the density and temperature profiles are radially well separated. Figure 10 exhibits the radial eigenfunction ($|\tilde{n}_i|^2$) for the lowest radial mode ($\ell=1$, $h=1$, $k_\parallel=\pi/L$) obtained in such a case. It is seen that the eigenfunction has two well-separated peaks that are not located at the positions where the gradients in density and temperature have their largest value. The inherent distortion in the eigenfunction can be misinterpreted in an experiment as being a higher radial mode or the consequence of a nonlinear interaction. The eigenfrequency of this mode is $\approx$50 kHz, which is to be compared with the eigenfrequency ($\approx$56 kHz), from Figs. 8 and 9 of a mode in which the two gradients are not radially separated.

IV. COMPARISON TO EXPERIMENT

In the LAPD experiment[16,17] the frequency spectrum of density and magnetic fluctuations spontaneously excited within a narrow striation has been measured. It is found that the density fluctuations exhibit relatively narrow peaks (eigenmodes) at frequencies lower than 50 kHz as the magnetic field if varied from 0.5 to 2.0 kG. The dominant peak has a frequency in the neighborhood of 37 ± 1 kHz (at 1 kG), which is fairly insensitive to substantial variations in operational parameters. To establish a quantitative comparison between the predictions of the present analysis and the experimental results, Fig. 11 displays the dependence of the calculated growth rate as a function of frequency for the lowest axial mode ($k_\parallel=\pi/L$); various combinations of azimuthal and radial (ℓ, h) mode numbers are included. The solid curve in Fig. 11 is the measured power spectrum (in log scale) of the density fluctuations. It is seen that indeed the dominant peak in the measured spectrum corresponds to the modes predicted to have the largest growth rates. The decrease in growth rate for modes having lower frequency is consistent with the general trend of the measured spectrum. However, the experimentally observed peak at 25 kHz does not have a theoretical counterpart. This implies that its origin is not a direct consequence of the linear physics of electrostatic drift waves.

The next comparison tests the shape of the radial eigenfunctions associated with the dominant peak at 37 kHz, as shown in Fig. 12. The solid curve is the theoretical prediction for the density fluctuation (i.e., $|\tilde{n}_i|^2$), calculated using Eq. (29) for a ($\ell=2$, $h=1$, $k_\parallel=\pi/L$) mode, which has the largest growth rate. The solid diamonds represent the fluctuations in the ion saturation current measured with a small probe. The open symbols denote experimental measurements of the scaled density and electron temperature profiles of the striation; the solid curves passing through these symbols are the analytical fits used in solving Eq. (8). The excellent agreement found between the theoretical density eigenfunction and the measurements indicate that the dominant peak excited in the striation (at 1 kG) is predominantly an electrostatic drift wave.

In the LAPD experiment it is observed that the dominant

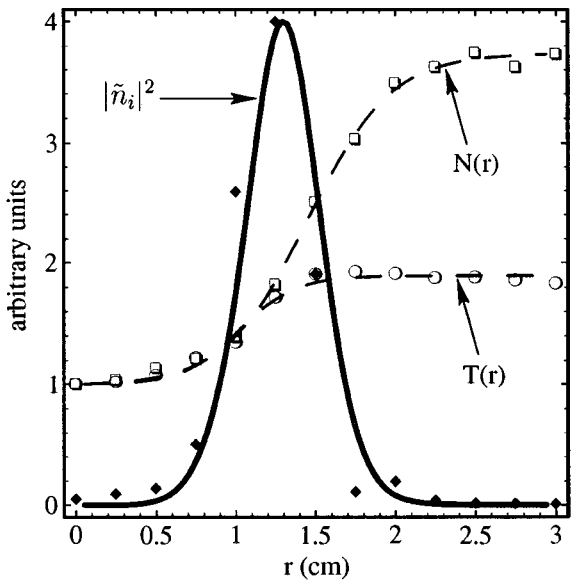

FIG. 12. A theoretical prediction (solid curve) of the radial profile of density fluctuations corresponding to the largest growth rate. Solid diamonds are the experimental measurements corresponding to the dominant peak at 37 kHz. Circles are measurements of electron temperature and squares are plasma density. Dashed lines through these data points represent analytical fits used in theoretical calculation.

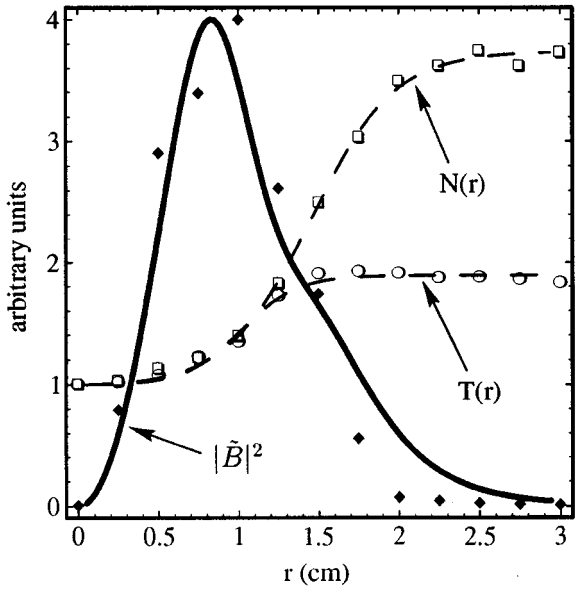

FIG. 13. Solid curve corresponds to calculated radial dependence of magnetic fluctuation ($|\tilde{B}|^2$) accompanying the radial density eigenfunction of Fig. 12. Solid diamonds are measured values.

peak at 37 ± 1 kHz exhibits both density and magnetic fluctuations. Since the lowest frequency of an axially standing shear Alfvén wave ($\omega/2\pi=v_A/2L$, where v_A is the Alfvén speed) is close to 37 kHz the dominant mode should be more appropriately described as a drift-Alfvén wave. However, since the frequency of the mode and the density eigenfunction are well described by an electrostatic theory, it is of interest to test if the shape of the magnetic eigenfunction can be obtained from an iterative analysis.

To obtain a fluctuating magnetic field it is useful to recognize that the ratio of the parallel displacement current $j_\parallel^D$ to the parallel electrical current $j_\parallel$ (carried by the electrons) is

$$\frac{|\tilde{j}_\parallel^D|}{|\tilde{j}_\parallel|}=\left(\frac{k_\parallel}{k_D}\right)^2 \times\frac{1}{|Z_N(W,\rho)/2T(\rho)+(\ell/\rho)(1-\lambda^2W)\Gamma(W,\rho)|}, \tag{30}$$

where k_D is the Debye number at the center of the striation, and the results of the electrostatic calculation obtained by setting $\tilde{n}_e\approx\tilde{n}_i$ are used. In the relevant limit in which $k_\parallel\ll k_D$ the displacement current can be neglected in the parallel component of Ampère's law (as is common practice in describing Alfvén waves) to yield

$$\frac{1}{r}\frac{\partial}{\partial r}(r\tilde{B}_\theta)-\frac{\iota\ell}{r}\tilde{B}_r=\frac{4\pi}{c}\tilde{j}_\parallel, \tag{31}$$

where $\tilde{B}_r$, $\tilde{B}_\theta$ are the (r,θ) components of the magnetic fluctuations, and $j_\parallel=-e(\omega/k_\parallel)\tilde{n}_i$ with $\tilde{n}_i$ obtained from Eq. (5). Assuming a shear wave polarization (i.e., $\tilde{B}_\parallel$ is negligible) and using $\nabla\cdot\tilde{B}=0$ yields

$$\tilde{B}_\theta(r)=\frac{\iota}{\ell}\frac{\partial}{\partial r}[r\tilde{B}_r(r)], \tag{32}$$

which makes Eq. (31) take the form

$$\frac{1}{r}\frac{\partial}{\partial r}\left[r\frac{\partial}{\partial r}(r\tilde{B}_r)\right]-\frac{\ell^2}{r}\tilde{B}_r=-\frac{4\pi}{c}\iota\ell\tilde{j}_\parallel(r). \tag{33}$$

Using the appropriate Green's functions results in

$$\tilde{B}_r(r)=\frac{2\pi\iota}{c}\left(\frac{1}{r^{\ell+1}}\int_0^r d\xi\ \xi^{l+1}\tilde{j}_\parallel(\xi) + r^{\ell-1}\int_r^\infty d\xi\ \xi^{1-\ell}\tilde{j}_\parallel(\xi)\right), \tag{34}$$

from which $\tilde{B}_\theta$ can be obtained according to Eq. (32).

The solid curve in Fig. 13 displays the radial dependence of the fluctuating magnetic field (i.e., $|\tilde{B}|^2$) predicted by the iterative analysis for the same mode ($\ell=2$, $h=1$, $k_\parallel=\pi/L$) whose density eigenfunction is shown in Fig. 12. The solid diamonds are the measured values (in arbitrary units) obtained with a small magnetic induction loop. It is found that the predicted shape of the magnetic fluctuations is in good agreement with the observations.

V. DISCUSSION

A formulation has been presented of the eigenvalue problem for electrostatic drift waves trapped within narrow filamentary depletions in plasma density and electron temperature in an infinite plasma. The linear behavior of the drift waves in a collisional plasma described by a Lorentz colli-

sion operator has been compared to that obtained in the collisionless regime. In general, the eigenfrequencies of the collisional plasma are found to be smaller than those predicted by the collisionless description. Although no simple trend is found for the growth rate, the collisional plasma tends to exhibit a broader range of instability (e.g., as the magnetic field is changed) than predicted by collisionless theory.

The numerical study of the eigenvalue problem has focused on conditions relevant to a laboratory experiment conducted in the large plasma device (LAPD) at UCLA in which the spontaneous fluctuations of a controlled striation have been measured. However, the range of parameter values considered when scaled to the relevant physical quantities (e.g., ω/Ω_i, $L_N\omega_{pe}/c$, etc.) are characteristic of those encountered in the auroral ionosphere.

As expected, the predictions of local theory, as illustrated by Fig. 3, are not useful in providing a quantitative explanation for the observed behavior. For instance, local theory predicts a frequency for the largest growth rate that is a factor 2 larger than obtained from the full-wave analysis.

A significant prediction of this theoretical study is that, for the collisional regime of relevance to the LAPD experiment, the frequency of the modes having the largest parallel wavelength in the device (i.e., $k_\parallel=\pi/L$) remains below 55 kHz over a broad range of parameter variations, as documented by Figs. 7–9. Indeed, it is a key experimental observation that the density eigenmodes appear only at frequencies below 55 kHz. Furthermore, as the control parameters of the experiment are varied (hence resulting in different density and temperature contrasts), the frequency of the mode having the largest density fluctuations exhibits relatively small changes. This behavior is well explained by the weak dependence on magnetic field (Fig. 7), temperature contrast (Fig. 8), and density contrast (Fig. 9) exhibited by the calculated eigenfrequencies.

A characteristic behavior observed in the experiment is that when the primary current pulse is terminated the temperature profile of the plasma decays rapidly while the density profile remains relatively unchanged. Accompanying the temperature decay it is observed that the fluctuation amplitude decays while simultaneously the frequency associated with the fluctuation decreases. This behavior is consistent with the predicted dependence on the temperature contrast presented in Fig. 8. That is, as the heat source provided by the discharge current is removed, the temperature outside the striation drops rapidly and results in a flat temperature profile and subsequently lower eigenfrequencies and lower growth rates. During the rapid temperature decay the density profile remains unchanged basically due to ion inertia.

Since the present detailed analysis is highly successful in explaining some features of the dominant density fluctuations observed in the laboratory, it is extremely valuable to highlight the areas of discrepancy between theory and observation because they signal the presence of new physical processes that require further experimentation and analysis. From the predicted dependence of the growth rate on $k_\parallel$ for different $\not{\ell}$ numbers, as shown in Fig. 6, it is anticipated that significant eigenmodes should be excited with $k_\parallel=(2-3)\pi/L$. The corresponding frequencies, however, are in the range of 60–70 kHz and are not observed in the experiment. This implies that there is some mechanism suppressing the growth of higher $k_\parallel$ modes. The mechanism is probably associated with the finite length of the device. In this regard it is interesting to note from Figs. 5 and 6 that, the axial group velocity, $v_g=\partial\omega/\partial k_\parallel$ is largest in the small $k_\parallel$ region, having a value intermediate between the ion sound speed and the Alfvén velocity, $c_s \ll v_g \ll v_A$. This behavior suggests that the time scale associated with energy transport along the device axis may play the determining role in selecting which wavelength grows. The suppression of higher $k_\parallel$ modes is a feature consistently observed in previous drift-wave experiments[22–25] in finite length devices, although no satisfactory theoretical description for this behavior is presently available. Noteworthy attempts to incorporate the effect of finite axial extent are found in the study by Tsai *et al.*,[26] and more recently in a global analysis (in one dimension) by Schupfer *et al.*[27]

Another interesting anomaly is associated with the theoretical prediction illustrated in Figs. 8 and 9 that the density gradient is the primary driver for the drift-wave instability. The mode with the largest growth rate stabilizes as the density profile flattens. However, Fig. 8 indicates that even with a flat electron temperature profile there still exists significant wave growth in the presence of a density gradient. In contrast, the experimental evidence is that in the afterglow plasmas in which the temperature profile is flat, but the density gradients remain, the instability disappears. Apparently some loss mechanism, not accounted for in the theory, is operating in the LAPD plasma. This effect may again be due to the finite length of the device and be associated with energy loss processes occurring at the ends of the plasma column.

Finally, the clear eigenmode experimentally observed at 25 kHz, as shown in Fig. 11, in a band where no eigenmodes are predicted to exist using electrostatic theory clearly indicates that a fundamental physical process is missing from the analysis. There are three possibilities that are worthy of serious consideration: additional electrostatic modes associated with azimuthal rotation due to a dc radial electric field: a different eigenmode structure associated with drift-Alfvén waves becoming more prominent at lower frequencies; and nonlinear beat-coupling driven by the large-amplitude oscillation at 37 kHz.

In summary, a significant understanding has been achieved of the properties of electrostatic drift waves trapped within a narrow filament. However, a detailed quantitative comparison with experimental observations has identified several unexplained effects that warrant future investigation.

ACKNOWLEDGMENT

This work is sponsored by the Office of Naval Research.

[1] A. Mikhailovsky, in *Handbook of Plasma Physics*, edited by M. Rosenbluth and R. Sagdeev (North-Holland, New York, 1984), Vol. 1, p. 587.
[2] W. Horton, in Ref. 1, Vol. 2, p. 384.
[3] R. F. Ellis and E. Marden-Marshall, Phys. Fluids **22**, 2137 (1979).
[4] U. Kauschke, G. Oelerich-Hill, and A. Piel, Phys. Fluids B **2**, 38 (1989).
[5] J. B. Taylor, Phys. Fluids B **5**, 4378 (1993).
[6] J. F. Drake, R. G. Kleva, and M. E. Mandt, Phys. Rev. Lett. **73**, 1251 (1994).

[7]R. G. Kleva, Phys. Rev. Lett. **73**, 1509 (1994).
[8]R. Kinney, T. Tajima, J. C. McWilliams, and N. Petviashvili, Phys. Plasmas **1**, 260 (1994).
[9]S. J. Zweben and S. S. Medley, Phys. Fluids B **1**, 2058 (1989).
[10]N. J. L. Cardozo, F. C. Schuller, C. J. Barth, C. C. Chu, F. J. Pipjer, J. Lok, and A. A. Oomeus, Phys. Rev. Lett. **73**, 256 (1994).
[11]G. Morales and H. Ramachandran, in *International Conference on Plasma Physics* (European Physical Society, Petit-Lancy, Switzerland, 1992), Vol. 16C, pp. 1–135.
[12]M. Kelly, T. Arce, J. Salowey, M. Sulzer, W. Armstrong, M. Carter, and L. Duncan, J. Geophys. Res. **100**, 367 (1995).
[13]P. Kintner, J. Vago, S. Chesney, R. Arnoldy, K. Lynch, C. Pollock, and T. Moore, Phys. Rev. Lett. **68**, 2448 (1992).
[14]A. Erikkson, B. Holback, P. Dovner, R. Bostrom, G. Homgren, M. Andre, L. Eliasson, and P. Kintner, Geophys. Res. Lett. **71**, 2409 (1993).
[15]P. Muralikrishna and M. Abdu, J. Atmos. Terr. Phys. **53**, 787 (1991).
[16]J. E. Maggs and G. J. Morales, Geophys. Res. Lett. **23**, 633 (1996).
[17]J. E. Maggs and G. J. Morales, Phys. Plasmas **4**, 290 (1997).
[18]W. Gekelman, H. Pfister, Z. Lucky, J. Bamber, D. Leneman, and J. E. Maggs, Rev. Sci. Instrum. **62**, 2875 (1991).
[19]G. Schmidt, in *Physics of High Temperature Plasmas*, 2nd ed. (Academic, New York, 1979), Chap. 10, p. 355.
[20]S. I. Braginski, in *Reviews of Plasma Physics*, edited by M. Leontovich (Consultants Bureau, New York, 1965), Vol. 1, p. 205.
[21]R. A. Koch and J. W. Horton, Phys. Fluids **18**, 861 (1975).
[22]S. Tokuda, T. Kamimura, and H. Ito, Phys. Soc. Jpn. **48**, 1722 (1980).
[23]R. F. Ellis and R. W. Motley, Phys. Fluids **17**, 582 (1974).
[24]J. T. Tang and J. N. C. Luhmann, Phys. Fluids **19**, 1935 (1976).
[25]E. Marden-Marshall, R. F. Ellis, and J. E. Walsh, Plasma Phys. Controlled Fusion **28**, 1461 (1986).
[26]T. Tsai, R. Ellis, and F. Perkins, Phys. Fluids **15**, 345 (1972).
[27]N. Schupfer, S. Kuhn, A. de Assis, and M. Santiago, in *Proceedings of the 1994 International Conference on Plasma Physics*, Foz do Iguacu, Brazil, 31 October–4 November 1994, edited by P. Sakanaka, E. D. Bosco, and M. Alves (American Institute of Physics, Woodbury, NY, 1995), Vol. 2, p. 143.